Suppressing Andreev Bound State Zero Bias Peaks Using a Strongly Dissipative Lead

Shan Zhang,[1] Zhichuan Wang,[2] Dong Pan[ORCID],[3] Hangzhe Li,[1] Shuai Lu[ORCID],[1] Zonglin Li,[1] Gu Zhang,[4]
Donghao Liu,[1] Zhan Cao,[4] Lei Liu[ORCID],[3] Lianjun Wen,[3] Dunyuan Liao,[3] Ran Zhuo,[3] Runan Shang,[4]
Dong E. Liu,[1,4,5,*] Jianhua Zhao[ORCID],[3,†] and Hao Zhang[ORCID][1,4,5,‡]

[1]*State Key Laboratory of Low Dimensional Quantum Physics, Department of Physics,*
Tsinghua University, Beijing 100084, China
[2]*Beijing National Laboratory for Condensed Matter Physics, Institute of Physics,*
Chinese Academy of Sciences, Beijing 100190, China
[3]*State Key Laboratory of Superlattices and Microstructures, Institute of Semiconductors,*
Chinese Academy of Sciences, P.O. Box 912, Beijing 100083, China
[4]*Beijing Academy of Quantum Information Sciences, 100193 Beijing, China*
[5]*Frontier Science Center for Quantum Information, 100084 Beijing, China*

Hybrid semiconductor-superconductor nanowires are predicted to host Majorana zero modes that induce zero-bias peaks (ZBPs) in tunneling conductance. ZBPs alone, however, are not sufficient evidence due to the ubiquitous presence of Andreev bound states. Here, we implement a strongly resistive normal lead in InAs-Al nanowire devices and show that most of the expected Andreev bound state–induced ZBPs can be suppressed, a phenomenon known as environmental Coulomb blockade. Our result is the first experimental demonstration of this dissipative interaction effect on Andreev bound states and can serve as a possible filter to narrow down the ZBP phase diagram in future Majorana searches.

Electron tunneling in a dissipative environment has been widely studied by probing the transport through a nanoscale tunnel junction in contact with resistive leads [1–7]. The tunneling electrons interact with the electromagnetic plasmon modes of this ohmic environment, resulting in a suppression of the tunneling conductance ($G \equiv dI/dV$) at low bias voltage (V) and temperature (T), a phenomenon known as "environmental Coulomb blockade" (ECB) or "dynamical Coulomb blockade." This phenomenon induces a characteristic power law in conductance as $G \propto \max(k_B T, eV)^{2r}$, similar as that in tunneling between two Luttinger liquid leads [8,9]. k_B is the Boltzmann constant and $r = R/(h/e^2)$ is the ratio between the lead resistance (R) and the quantum resistance (h/e^2). Later on, replacing the metallic tunnel junction with a semiconductor nanostructure, e.g., a quantum point contact [10,11] or a quantum dot [12–15], has significantly increased the system tunability and enabled various quantum phase transitions. For example, in a quantum dot with a single dot level resonantly coupled to the dissipative source and drain leads with the coupling strength being $\Gamma_{S/D}$, both experimental [13] and theoretical [15] studies have demonstrated that (1) in the asymmetric coupling regime ($\Gamma_S \neq \Gamma_D$), the Coulomb conductance peaks are significantly suppressed as T decreases, same as the typical ECB suppression; (2) in the symmetric coupling regime ($\Gamma_S = \Gamma_D$), the Coulomb peak height, to the contrary, increases as T decreases and finally saturates to the quantized conductance of e^2/h.

Motivated by this striking contrast, a theoretical study [16] has proposed a strongly dissipative lead being implemented in hybrid semiconductor-superconductor nanowires to identify signatures of Majorana zero modes (MZMs) [17–20]. Probing MZMs with a regular lead reveals zero-bias peaks (ZBPs) in tunneling conductance. The quantitative behavior of ZBPs observed in experiments [21–26], however, does not fully follow theoretical predictions. For example, the perfect Majorana quantization [27,28] has not been observed yet. This quantization is enabled by Andreev reflection where the injected electrons and Andreev reflected holes "see" the same barrier, similar to a quantum dot with symmetric resonant tunneling ($\Gamma_S = \Gamma_D$), leading to perfect transmission (ZBP quantization). Meanwhile, the biggest challenge of "Majorana hunting" comes from the coexistence of Andreev bound states (ABSs) in the same system [29]. These ABS-induced ZBPs, superficially similar to MZM signatures, can easily emerge due to potential inhomogeneity [30–33] or disorder [34–38], which cannot be currently eliminated [39,40]. The ABS conductance usually has different tunnel couplings for electrons and holes, similar to a quantum dot with asymmetric coupling ($\Gamma_S \neq \Gamma_D$), resulting in nonquantized ZBPs. Following the dissipative dot model, a strongly dissipative lead could suppress the ubiquitous ABS-induced ZBPs (asymmetric coupling) at low T, while the quantized ZBPs (symmetric coupling) should still survive as long as $r < 1/2$ [16].

In this Letter, we engineer such a dissipative lead in hybrid InAs-Al devices and demonstrate that strong dissipation can indeed suppress most ZBPs resulting from zero-energy ABSs. The survival of quantized ZBPs, possibly due to MZMs or quasi-MZMs [41,42], will be studied in the future.

Figure 1(a) shows a scanning electron microscope (SEM) image of the device (Device A). The Cr/Au film (red) was made thin and resistive, serving as an ohmic dissipative environment (referred as "dissipative resistor"). This resistor is connected to the InAs-Al nanowire through the Ti/Au contacting lead (yellow), which is made thick and negligible in resistance. The resistance of the dissipative resistor is estimated to be $\sim$5.7 kΩ based on independent calibration (see Fig. S1 in Ref. [43] for details). A total bias voltage V_{bias} is applied to the left lead. The current I,

(a)

Device A   1 um

InAs (38 nm)
Al (7 nm)
Cr/Au (10/2 nm)
Ti/Au (5/70 nm)

TG   300 nm

(b) Device A
$B_\perp = 1$ T
$V_{BG} = -3.08$ V
$V_{TG} = -5.625$ V

T (K)
1.190
0.800
0.532
0.412
0.325
0.261
0.210
0.171
0.138
0.107
0.083
0.057
0.042
0.028

(c) $r = 0.21$ Device A $r = 0.21$

(d) Device B $r = 0.37$ $B_\perp = 1$ T $V_{BG} = -1.792$ V

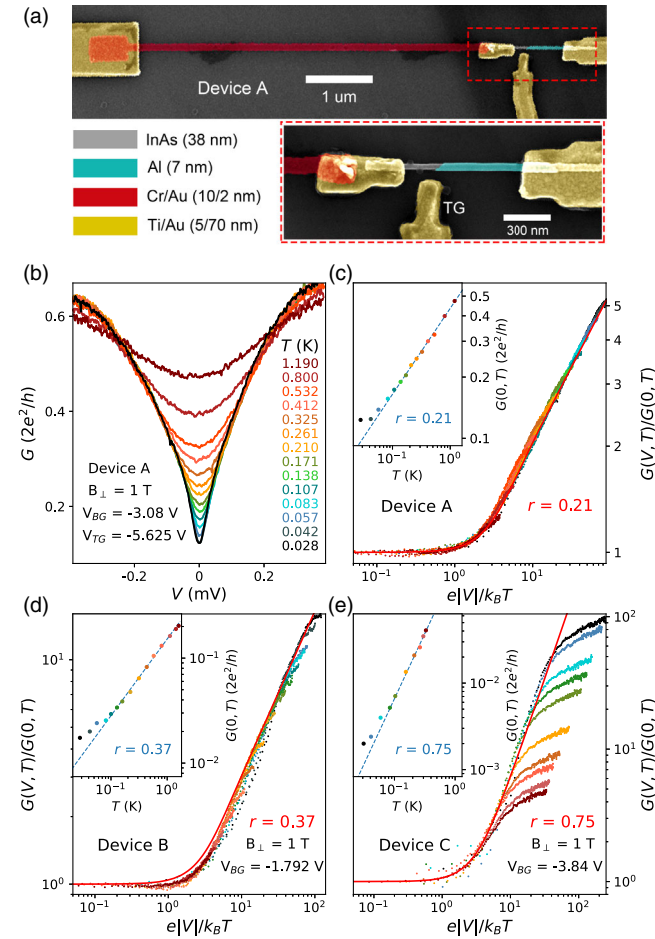(e) Device C $r = 0.75$ $B_\perp = 1$ T $V_{BG} = -3.84$ V

FIG. 1. (a) False-color SEM image of Device A. Thickness of the dissipative resistor (red), contact or gate (yellow), and InAs (diameter) are labeled. The substrate is p-doped Si covered by 300 nm thick SiO$_2$, acting as a global back gate. (b) $G(V,T)$ of device A at different Ts. $B_\perp = 1$ T. (c) Replotting (b) using dimensionless units. Inset: T dependence of the zero-bias G. (d) and (e) are for Devices B and C with different dissipative resistors.

after flowing through the dissipative resistor and the InAs-Al device, is drained and measured at the right contact. Differential conductance G is then calculated after subtracting the series resistance, R_{series}, which includes the dissipative resistor and the fridge filters. The bias V across the InAs-Al device is calibrated by subtracting the voltage drop shared on R_{series}: $V = V_{bias} - I \times R_{series}$. Therefore, $G = [1/(dV/dI)] = [1/(dV_{bias}/dI - R_{series})]$. The tunnel gate ($V_{TG}$) tunes the tunnel barrier in InAs, while the global back gate (V_{BG}) tunes both the barrier and the superconducting nanowire region. The dissipative resistor should be on chip and close to the InAs-Al device to guarantee significant ECB: if their physical distance were too large, the effect of ECB would decay and finally disappear, in which case the resistor would then behave like the fridge filters.

To demonstrate ECB, we first apply an out-of-plane magnetic field (B) of 1 T (perpendicular to the Al film) to suppress its superconductivity. The InAs-Al part is then equivalent to a normal tunnel junction. Figure 1(b) shows the significant suppression of G at low V and T, consistent with the hallmark of ECB. In Fig. 1(c), we rescale the data of Fig. 1(b) (the negative bias branch) using dimensionless units, where all curves collapse onto a single universal curve [the red line in Fig. 1(c)] with minor deviations. The red line is obtained via numerical differentiation of the current through a dissipative tunneling barrier [13]: $I(V,T) \propto V T^{2r} |\Gamma(r+1+ieV/2\pi k_B T)/\Gamma(1+ieV/2\pi k_B T)|^2$, where Γ is the Gamma function. The dissipation strength r is extracted from $G \propto T^{2r}$ at zero-bias (Fig. 1(c) inset). For $T < 100$ mK, G deviates from the power law (blue line), suggesting a gradual saturation of the electron T: fridge T of $\sim$30 mK roughly corresponds to an electron $T \sim 50$ mK. We use the electron T, estimated based on this "power-law" thermometer [44], for the rescaled x axis $e|V|/k_B T$ in Fig. 1 (c) for curves of $T < 100$ mK.

The dissipation strength, $r = 0.21$, translates to an effective resistance $r \times h/e^2 = 5.42$ kΩ, roughly consistent with our independent estimation of the dissipative resistor $\sim$5.7 kΩ. We have also checked similar power laws in Devices B and C, designed with larger dissipative resistors as shown in Figs. 1(d) and 1(e). The extracted exponent $r = 0.37$ (0.75) for Device B (C) corresponds to an effective resistance of 9.55(19.36) kΩ, also roughly consistent with our independent estimation of 7.5(27.28) kΩ. The deviations could be due to inaccurate estimations of the dissipative resistor (see Fig. S2 in Ref. [43]) or contributions from other dissipation sources. When the dissipative resistor R is comparable to the resistance of the tunneling junction (R_T), the effective R should be replaced by $1/(1/R + 1/R_T)$ [45], also causing deviations. Power-law fits at the other gate voltages (see Fig. S3 in Ref. [43]) show fluctuations possibly due to reasons mentioned above. In Fig. 1(e), G at larger bias deviates from the universal red line. This deviation, also

expected for Devices A and B for larger bias, is related to the power law being only valid within a finite energy bandwidth [7].

For comparison we have also tested and confirmed that a regular InAs-Al nanowire device without the dissipative resistor (Device X) does not show such ECB power-law suppression (see Fig. S4 in Ref. [43]).

We now set $B = 0$ T and study the dissipative tunneling into a superconductor in Device A. In the literature on "Majorana nanowires," the term "dissipation" usually refers to interface disorder and soft induced superconducting gaps [46,47]. To avoid confusion, in this Letter we refer "dissipation" only to effects caused by the dissipative resistor. In fact, we have shown the atomically abrupt InAs-Al interface [48], hard gaps, and large ZBPs [26] in these InAs-Al devices without dissipation. Now with the dissipative resistor (Device A), the gap is still hard, together with the existence of Coulomb blockade (see Fig. S5 in Ref. [43]). But the coherence peaks are smeared, possibly due to nonequilibrium dissipation. Nevertheless, we can still resolve clean ABS levels as shown in Fig. 2.

Figure 2(a) shows the gate dependence of an ABS. The two subgap levels do not cross, suggesting a singlet ground state [29]. Applying B parallel to the nanowire Zeeman splits the two peaks and drives the inner peaks toward zero

as shown in Figs. 2(b) and 2(c) (the splitting and the outer peaks are sometimes barely visible). In regular devices without dissipation, further increasing B can lead to level crossing and ZBP formation as shown in Fig. 2(h) for Device X. This ZBP, resulting from ABS level crossing, is ubiquitous and its underlying physics is well established [29,48]. Now back to our Device A with dissipation; in Figs. 2(b) and 2(c), the expected crossing points (arrows; see also Fig. S6 in Ref. [43] for "waterfall" plots) show significant suppression of zero-bias G and resolve split peaks instead of ZBPs. This zero-bias peak being suppressed to zero-bias valley (or split peaks) in devices with a strongly dissipative lead is the main observation of this Letter. We attribute this observation to the electron-boson interaction effect caused by the dissipative lead. ECB suppresses G in a nonuniform way: the suppression is stronger for lower T and V. Therefore, the zero-bias G at base T is suppressed the most, while the high-bias G is less affected, leading to the splitting of ZBPs [16].

Figure 2(d) shows another ABS whose ground state can be tuned from singlet (S) to doublet (D) continuously. At the parity switching point (arrow), the levels are expected to cross and form a ZBP for a regular nondissipative device. Here with dissipation, the "expected" ZBP is again suppressed. Figures 2(e) and 2(f) show the B dependence of the ABSs. For the singlet case [Fig. 2(e)], the two peaks merge towards zero energy (black arrow) where the "expected" ZBP is suppressed. In Fig. 2(f), the two peaks move away from zero energy, being consistent with the doublet behavior [29]. For additional B and gate scans of the ABSs in Figs. 2(a)–2(f), see Figs. S7 and S8 in Ref. [43].

For comparison, we show a ZBP data set in the control Device X (without the dissipative resistor) in Figs. 2(g) and 2(h). The ZBP, formed by merging of two ABS levels, shows some robustness (nonsplitting) in gate [Fig. 2(g)] and B [Fig. 2(h)] scans. The ZBP is not quantized, ruling out its topological origin; see Fig. S9 in Ref. [43] for additional scans. Figure 2(i) shows line cuts to contrast suppressed ZBPs in Device A (black) and ZBPs in Device X (red).

We now study the T dependence of the ABS in the presence of dissipation. Figure 3(a) shows the ABS from Fig. 2(d) at $B = 0.3$ T, measured at base T and at higher Ts. Figure 3(b) shows a near-zero energy ABS line cut from Fig. 3(a) measured at different Ts (only four shown for clarity). The solid lines are theory simulations using the formula $G(V, T) = \int_{-\infty}^{+\infty} G(\epsilon, 0)\{[\partial f(eV - \epsilon, T)]/\partial\epsilon\}d\epsilon$, where $f(E, T) = [1/(e^{E/k_BT} + 1)]$ is the Fermi distribution function. Note the unit eV in $G(V, T)$ is converted to ϵ in $G(\epsilon, 0)$ for convenience. We replace $G(\epsilon, 0)$ with the measured curve $G(V, T = 20 \text{ mK})$ to obtain $G(V, T)$. This assumption should be valid for T much larger than 20 mK in interaction-free systems. This "thermal broadening" simulation shows significant deviations from the experimental data, suggesting that thermal averaging alone
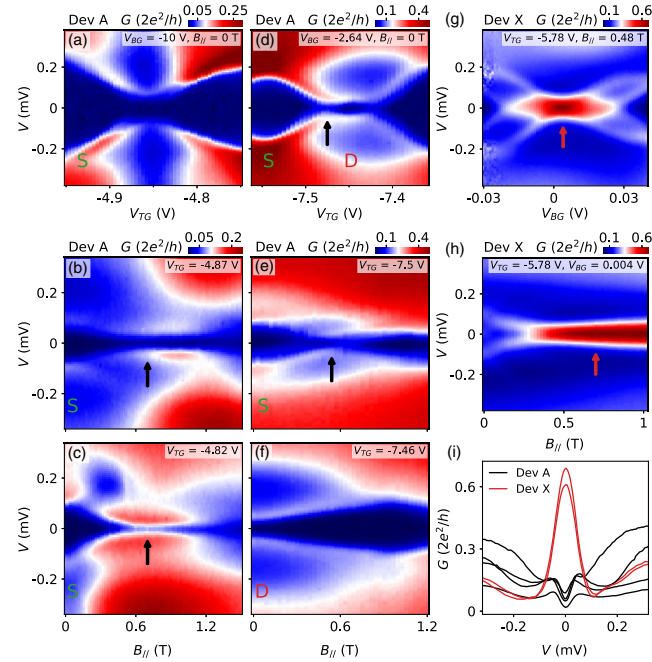
FIG. 2. (a)–(f) For Device A. (a) V_{TG} scan of a singlet ABS at $B = 0$ T. (b),(c) B scans of the ABS from (a) (V_{TG} labeled). (d) V_{TG} scan of another ABS at $B = 0$ T with singlet (S) and doublet (D) regions labeled. (e),(f) B scans of the singlet and doublet ABSs. (g),(h) Gate and B scans of an ABS in Device X (without dissipation). (i) Black and red curves are line cuts from (b)–(e) and (g),(h), respectively (see corresponding arrows). B is aligned with the nanowire axis. $T \sim 20$ mK.
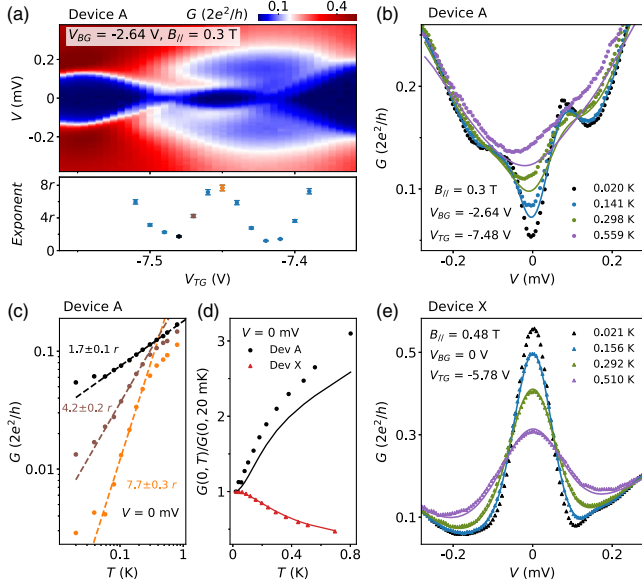
FIG. 3. (a) Upper, gate scan of an ABS at 0.3 T. $T \sim 20$ mK. Lower, extracted power-law exponents from T dependence in units of r. (b) T dependence (colored dots) of a line cut in (a). The solid lines are theory simulations. (c) T dependence of the zero-bias G from (a) at three V_{TG}s, labeled in the lower panel (a). Dashed lines are the power-law fits. (d) T dependence of the normalized zero-bias G from (b) for Device A (black dots) and Device X (red dots), together with thermal simulations (solid lines). (e) T dependence of a ZBP [from Fig. 2(g)] in Device X (dots) and thermal simulations (lines).

cannot explain the T dependence of the near zero-energy ABS. The measured G being larger than the simulated one also suggests the lifting of ECB suppression at higher Ts.

We further plot the zero-bias G for all Ts in Fig. 3(c) (black dots), and find a power law in T with an exponent of $(1.7 \pm 0.1)r$, assuming $r = 0.22 \pm 0.01$. At other gate voltages where the ABS has finite energies, we also find similar power-law-like behavior over an intermediate T range (from $\sim$60 to $\sim$300 mK); see the brown and orange dots with exponents of $(4.2 \pm 0.2)r$ and $(7.7 \pm 0.3)r$. Figure 3(a) (lower panel) shows all the extracted exponents (for the left- and right-most regions, we cannot find reasonable power-law-like fits). For more T dependence, see Fig. S10 in Ref. [43].

Recently [49], we have theoretically studied dissipative tunneling mediated by Andreev reflection and showed that the power-law exponent can be $8r$ or $4r$, corresponding to coherent or incoherent processes. Other exponent values between $8r$, $4r$, and $2r$ (normal tunneling) could also be achieved depending on their mixing. Our observation here shows some consistency with the theory but still requires further systematic study. For example, we note the power law T range in Fig. 3(c) is not large (only half a decade). For $T < 60$ mK, the deviation between the data and the power law is possibly due to the saturation of electron T. For $T > 300$ mK, the deviation is probably due to gap

softening or quasiparticle poisoning where incoherent Andreev reflection or normal tunneling contributes. Nevertheless, optimizations are needed for better power-law fits to fully understand "dissipative Andreev tunneling."

In Fig. 3(d), we replot the black dots from Fig. 3(c), deviating significantly from the thermal simulation (the black line). By contrast, T dependence of ZBPs in the control Device X shows reasonable agreement with the simulation for both zero bias (Fig. 3(d), red) and finite bias [Fig. 3(e)], suggesting that thermal averaging is indeed the dominating effect in the T evolution of zero-energy ABS in Device X. This sharp contrast between Figs. 3(b) and 3(e) confirms the Fermi liquid T dependence in Device X (without dissipation) and suggests the non-Fermi liquid T dependence in Device A (with dissipation). The gap softening at higher Ts, not included in the simulation, could cause small deviations between data and simulation in Device X, especially for nonzero energy ABSs (see Fig. S9 in Ref. [43]). Therefore, we restrict our thermal simulation to only zero or near-zero energy ABSs.

We have shown several expected ZBPs being suppressed by dissipation in Fig. 2. In fact, almost all ZBPs in Device A are suppressed within the explored parameter space. Figure 4(a) shows the zero-bias G over a large gate scan at 1 T where ZBPs are otherwise likely to occur [26]. The dense diagonal lines suggest possible formations of quantum dots and ABSs. Further bias scan [Fig. 4(b)], however, resolves no ZBPs [see Fig. 4(c)]. We have also checked many other regions in the parameter space of Device A, and did not find clear ZBPs (see Fig. S11 in Ref. [43]). This absence of ZBP is dramatically different from our previous experience where ZBPs can be easily and routinely found
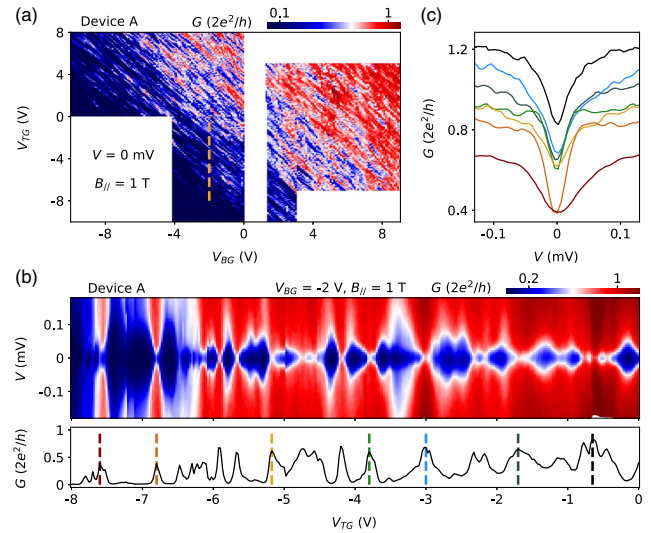

FIG. 4. (a) Zero-bias G at 1 T (aligned with the nanowire) versus V_{BG} and V_{TG}. (b) G versus V_{TG} and V. Lower panel zero-bias line cut, corresponding to the orange dashed line in (a). (c) Vertical line cuts from (b); see colored dashed lines, resolving no ZBPs. $T \sim 20$ mK.

in dissipation-free devices [26,48]. Very rarely, faint and small ZBP-like features can be barely visible; see Fig. S11 in Ref. [43] for the only such case found in Device A. For Devices B and C, we did not find any ZBP (see Fig. S5 in Ref. [43]). We note that this observation is consistent with our expectation since in regular devices: (1) nonquantized ZBPs are ubiquitous in every device [50]; (2) large (nearly quantized) ZBPs are rare and not in every device [25,26].

We finally remark that the dissipation strength r is a crucial parameter. If r is too strong (larger than $1/2$), theory [16] predicts that all ZBPs (including Majoranas) will be suppressed. If r is less than $1/2$, (quasi-) Majorana ZBPs could survive while trivial ZBPs will be suppressed (the latter demonstrated in this Letter). But r cannot be arbitrarily small. For example, if r is approaching zero (Device X), apparently trivial ZBPs will revive. We identify $r \geq 0.22$ as the strong dissipative regime based on the observation that most of ABS-induced ZBPs are suppressed.

To summarize, we have implemented a strongly dissipative lead in InAs-Al hybrid nanowire devices. The dissipative environment, confirmed by the observation of ECB with power laws and non-Fermi liquid T dependence, can significantly suppress the ABS-induced ZBPs, which ubiquitously exist and disturb Majorana detections. Our result could serve as a possible filter to narrow down the ZBP phase diagram in future Majorana searches [16,49,51–54].

*Corresponding author.
dongeliu@mail.tsinghua.edu.cn
†Corresponding author.
jhzhao@semi.ac.cn
‡Corresponding author.
hzquantum@mail.tsinghua.edu.cn

[1] P. Delsing, K. K. Likharev, L. S. Kuzmin, and T. Claeson, Effect of High-Frequency Electrodynamic Environment on the Single-Electron Tunneling in Ultrasmall Junctions, Phys. Rev. Lett. 63, 1180 (1989).

[2] M. H. Devoret, D. Esteve, H. Grabert, G.-L. Ingold, H. Pothier, and C. Urbina, Effect of the Electromagnetic Environment on the Coulomb Blockade in Ultrasmall Tunnel Junctions, Phys. Rev. Lett. 64, 1824 (1990).

[3] A. N. Cleland, J. M. Schmidt, and J. Clarke, Charge Fluctuations in Small-Capacitance Junctions, Phys. Rev. Lett. 64, 1565 (1990).

[4] G. L. Ingold and Y. V. Nazarov, Single Charge Tunnelling: Coulomb Blockade Phenomena in Nanostructures, edited by H. Grabert and M. H. Devoret (Springer, New York, 1992), pp. 21–107.

[5] K. Flensberg, S. M. Girvin, M. Jonson, D. R. Penn, and M. D. Stiles, Quantum mechanics of the electromagnetic environment in the single-junction coulomb blockade, Phys. Scr. T42, 189 (1992).

[6] P. Joyez, D. Esteve, and M. H. Devoret, How is the Coulomb Blockade Suppressed in High-Conductance Tunnel Junctions?, Phys. Rev. Lett. 80, 1956 (1998).

[7] W. Zheng, J. Friedman, D. Averin, S. Han, and J. Lukens, Observation of strong coulomb blockade in resistively isolated tunnel junctions, Solid State Commun. 108, 839 (1998).

[8] A. M. Chang, Chiral Luttinger liquids at the fractional quantum Hall edge, Rev. Mod. Phys. 75, 1449 (2003).

[9] I. Safi and H. Saleur, One-Channel Conductor in an Ohmic Environment: Mapping to a Tomonaga-Luttinger Liquid and Full Counting Statistics, Phys. Rev. Lett. 93, 126602 (2004).

[10] S. Jezouin, M. Albert, F. Parmentier, A. Anthore, U. Gennser, A. Cavanna, I. Safi, and F. Pierre, Tomonaga–Luttinger physics in electronic quantum circuits, Nat. Commun. 4, 1802 (2013).

[11] A. Anthore, Z. Iftikhar, E. Boulat, F. D. Parmentier, A. Cavanna, A. Ouerghi, U. Gennser, and F. Pierre, Circuit Quantum Simulation of a Tomonaga-Luttinger Liquid with an Impurity, Phys. Rev. X 8, 031075 (2018).

[12] Y. Bomze, H. Mebrahtu, I. Borzenets, A. Makarovski, and G. Finkelstein, Resonant tunneling in a dissipative environment, Phys. Rev. B 79, 241402(R) (2009).

[13] H. T. Mebrahtu, I. V. Borzenets, D. E. Liu, H. Zheng, Y. V. Bomze, A. I. Smirnov, H. U. Baranger, and G. Finkelstein, Quantum phase transition in a resonant level coupled to interacting leads, Nature (London) 488, 61 (2012).

[14] H. Mebrahtu, I. Borzenets, H. Zheng, Y. V. Bomze, A. Smirnov, S. Florens, H. Baranger, and G. Finkelstein, Observation of Majorana quantum critical behaviour in a resonant level coupled to a dissipative environment, Nat. Phys. 9, 732 (2013).

[15] D. E. Liu, H. Zheng, G. Finkelstein, and H. U. Baranger, Tunable quantum phase transitions in a resonant level coupled to two dissipative baths, Phys. Rev. B 89, 085116 (2014).

[16] D. E. Liu, Proposed Method for Tunneling Spectroscopy with Ohmic Dissipation using Resistive Electrodes: A Possible Majorana Filter, Phys. Rev. Lett. 111, 207003 (2013).

[17] R. M. Lutchyn, J. D. Sau, and S. Das Sarma, Majorana Fermions and a Topological Phase Transition in Semiconductor-Superconductor Heterostructures, Phys. Rev. Lett. 105, 077001 (2010).

[18] Y. Oreg, G. Refael, and F. von Oppen, Helical Liquids and Majorana Bound States in Quantum Wires, Phys. Rev. Lett. 105, 177002 (2010).

[19] R. M. Lutchyn, E. P. Bakkers, L. P. Kouwenhoven, P. Krogstrup, C. M. Marcus, and Y. Oreg, Majorana zero

modes in superconductor–semiconductor heterostructures, Nat. Rev. Mater. **3**, 52 (2018).

[20] E. Prada, P. San-Jose, M. W. de Moor, A. Geresdi, E. J. Lee, J. Klinovaja, D. Loss, J. Nygård, R. Aguado, and L. P. Kouwenhoven, From Andreev to Majorana bound states in hybrid superconductor–semiconductor nanowires, Nat. Rev. Phys. **2**, 575 (2020).

[21] V. Mourik, K. Zuo, S. M. Frolov, S. Plissard, E. P. Bakkers, and L. P. Kouwenhoven, Signatures of Majorana fermions in hybrid superconductor-semiconductor nanowire devices, Science **336**, 1003 (2012).

[22] M. Deng, S. Vaitiekėnas, E. B. Hansen, J. Danon, M. Leijnse, K. Flensberg, J. Nygård, P. Krogstrup, and C. M. Marcus, Majorana bound state in a coupled quantum-dot hybrid-nanowire system, Science **354**, 1557 (2016).

[23] Ö. Gül, H. Zhang, J. D. Bommer, M. W. de Moor, D. Car, S. R. Plissard, E. P. Bakkers, A. Geresdi, K. Watanabe, T. Taniguchi, and L. P. Kouwenhoven, Ballistic Majorana nanowire devices, Nat. Nanotechnol. **13**, 192 (2018).

[24] F. Nichele, A. C. Drachmann, A. M. Whiticar, E. C. OFarrell, H. J. Suominen, A. Fornieri, T. Wang, G. C. Gardner, C. Thomas, A. T. Hatke, P. Krogstrup, M. J. Manfra, K. Flensberg, and C. M. Marcus, Scaling of Majorana Zero-Bias Conductance Peaks, Phys. Rev. Lett. **119**, 136803 (2017).

[25] H. Zhang *et al.*, Large zero-bias peaks in insb-al hybrid semiconductor-superconductor nanowire devices, arXiv:2101.11456.

[26] H. Song, Z. Zhang, D. Pan, D. Liu, Z. Wang, Z. Cao, L. Liu, L. Wen, D. Liao, R. Zhuo, D. E. Liu, R. Shang, J. Zhao, and H. Zhang, Large zero bias peaks and dips in a four-terminal thin InAs-Al nanowire device, arXiv:2107.08282.

[27] K. Sengupta, I. Žutić, H.-J. Kwon, V. M. Yakovenko, and S. Das Sarma, Midgap edge states and pairing symmetry of quasi-one-dimensional organic superconductors, Phys. Rev. B **63**, 144531 (2001).

[28] K. T. Law, P. A. Lee, and T. K. Ng, Majorana Fermion Induced Resonant Andreev Reflection, Phys. Rev. Lett. **103**, 237001 (2009).

[29] E. J. Lee, X. Jiang, M. Houzet, R. Aguado, C. M. Lieber, and S. De Franceschi, Spin-resolved Andreev levels and parity crossings in hybrid superconductor–semiconductor nanostructures, Nat. Nanotechnol. **9**, 79 (2014).

[30] E. Prada, P. San-Jose, and R. Aguado, Transport spectroscopy of N S nanowire junctions with majorana fermions, Phys. Rev. B **86**, 180503(R) (2012).

[31] G. Kells, D. Meidan, and P. Brouwer, Near-zero-energy end states in topologically trivial spin-orbit coupled superconducting nanowires with a smooth confinement, Phys. Rev. B **86**, 100503(R) (2012).

[32] C.-X. Liu, J. D. Sau, T. D. Stanescu, and S. Das Sarma, Andreev bound states versus Majorana bound states in quantum dot-nanowire-superconductor hybrid structures: Trivial versus topological zero-bias conductance peaks, Phys. Rev. B **96**, 075161 (2017).

[33] Z. Cao, H. Zhang, H.-F. Lü, W.-X. He, H.-Z. Lu, and X. C. Xie, Decays of Majorana or Andreev Oscillations Induced by Steplike Spin-Orbit Coupling, Phys. Rev. Lett. **122**, 147701 (2019).

[34] J. Liu, A. C. Potter, K. T. Law, and P. A. Lee, Zero-Bias Peaks in the Tunneling Conductance of Spin-Orbit-Coupled Superconducting Wires with and without Majorana End-States, Phys. Rev. Lett. **109**, 267002 (2012).

[35] D. E. Liu, E. Rossi, and R. M. Lutchyn, Impurity-induced states in superconducting heterostructures, Phys. Rev. B **97**, 161408(R) (2018).

[36] H. Pan and S. Das Sarma, Physical mechanisms for zero-bias conductance peaks in Majorana nanowires, Phys. Rev. Research **2**, 013377 (2020).

[37] H. Pan, C.-X. Liu, M. Wimmer, and S. Das Sarma, Quantized and unquantized zero-bias tunneling conductance peaks in Majorana nanowires: Conductance below and above $2e^2/h$, Phys. Rev. B **103**, 214502 (2021).

[38] S. Das Sarma and H. Pan, Disorder-induced zero-bias peaks in Majorana nanowires, Phys. Rev. B **103**, 195158 (2021).

[39] S. Ahn, H. Pan, B. Woods, T. D. Stanescu, and S. Das Sarma, Estimating disorder and its adverse effects in semiconductor Majorana nanowires, Phys. Rev. Mater. **5**, 124602 (2021).

[40] C. Zeng, G. Sharma, S. Tewari, and T. Stanescu, Partially-separated Majorana modes in a disordered medium, arXiv:2105.06469.

[41] A. Vuik, B. Nijholt, A. Akhmerov, and M. Wimmer, Reproducing topological properties with quasi-Majorana states, SciPost Phys. **7**, 061 (2019).

[42] C. Moore, C. Zeng, T. D. Stanescu, and S. Tewari, Quantized zero-bias conductance plateau in semiconductor-superconductor heterostructures without topological Majorana zero modes, Phys. Rev. B **98**, 155314 (2018).

[43] See Supplemental Material at http://link.aps.org/supplemental/10.1103/PhysRevLett.128.076803 for additional data and analysis.

[44] H. T. Mebrahtu, Electron transport through carbon nanotube quantum dots in a dissipative environment, Ph.D. thesis, Duke University, 2012.

[45] K. Flensberg and M. Jonson, Quantum fluctuations and charging effects in small tunnel junctions, Phys. Rev. B **43**, 7586 (1991).

[46] S. Takei, B. M. Fregoso, H.-Y. Hui, A. M. Lobos, and S. D. Sarma, Soft Superconducting Gap in Semiconductor Majorana Nanowires, Phys. Rev. Lett. **110**, 186803 (2013).

[47] C.-X. Liu, J. D. Sau, and S. Das Sarma, Role of dissipation in realistic majorana nanowires, Phys. Rev. B **95**, 054502 (2017).

[48] D. Pan, H. Song, S. Zhang, L. Liu, L. Wen, D. Liao, R. Zhuo, Z. Wang, Z. Zhang, S. Yang, J. Ying, W. Miao, R. Shang, H. Zhang, and J. Zhao, *In situ* epitaxy of pure phase ultra-thin InAs-Al nanowires for quantum devices, arXiv:2011.13620.

[49] D. Liu, G. Zhang, Z. Cao, H. Zhang, and D. E. Liu, preceding Letter, Universal Conductance Scaling of Andreev Reflections Using a Dissipative Probe, Phys. Rev. Lett. **128**, 076802 (2022).

[50] M. W. de Moor, J. D. Bommer, D. Xu, G. W. Winkler, A. E. Antipov, A. Bargerbos, G. Wang, N. Van Loo, R. L. O. het Veld, S. Gazibegovic *et al.*, Electric field tunable superconductor-semiconductor coupling in Majorana nanowires, New J. Phys. **20**, 103049 (2018).

[51] D. Liu, Z. Cao, H. Zhang, and D. E. Liu, Revealing the nonlocal coherent nature of Majorana devices from dissipative teleportation, Phys. Rev. B **101**, 081406(R) (2020).

[52] G. Zhang and C. Spånslätt, Distinguishing between topological and quasi Majorana zero modes with a dissipative resonant level, Phys. Rev. B **102**, 045111 (2020).

[53] S.-P. Chiu, C. Tsuei, S.-S. Yeh, F.-C. Zhang, S. Kirchner, and J.-J. Lin, Observation of triplet superconductivity in $CoSi_2$/$TiSi_2$ heterostructures, Sci. Adv. **7**, eabg6569 (2021).

[54] H. Zhang, D. E. Liu, M. Wimmer, and L. P. Kouwenhoven, Next steps of quantum transport in Majorana nanowire devices, Nat. Commun. **10**, 5128 (2019).

[55] S. Zhang *et al.*, Suppressing Andreev bound state zero bias peaks using a strongly dissipative lead (2021), 10.5281/zenodo.5968611.